ORIGINAL PAPER

Thermally activated mango peels hydrochar for fixed-bed continuous flow decontamination of Pb(II) ions from aqueous solution

I. K. Rind[1] · N. Memon[1] · M. Y. Khuhawar[2] · M. F. Lanjwani[3]

Abstract

Thermally activated hydrochars prepared from mango peels have been tested for continuous removal of lead ions from contaminated drinking water for possible use in point-of-use candle-type water filters. The hydrochar was obtained using low-temperature hydrothermal carbonization, which was activated at various temperatures to produce activated hydrochars. The materials have been characterized physicochemically according to ASTM standards for activated carbons. The structure and morphology were studied by FTIR, XRD, SEM and nitrogen adsorption porosimetry. The results obtained showed that hydrochar activated at 400 °C (ACH 400) was promising for the elimination of lead with a obtained equilibrium absorption capacity of 38.31 mg/g at the optimized height parameters of bed (2.4 cm), flow rate (12 mL/min) and lead concentration (100 mg/L). The results of the experimental breakthrough curves given by adsorption process were successfully fitted by kinetic models according to Adams–Bohart, Thomas and Yoon–Nelson in their linearized forms. The Thomas and Yoon-Nelson data provided a better correlation with the prediction of the breakthrough curve data with high R^2 values, showing a good agreement between the breakthrough curves and the experimental data points. ACH 400 is a suitable sorbent in place of activated carbon for a continuous system and can be applied for large-scale treatment for the removal of lead from water samples.

Keywords Activated hydrochar · Lead ion decontamination · Low-temperature carbonization · Fixed-bed column · Point-of-use filtration

Introduction

Surface waters are found contaminated with unwanted metal ions at many places on earth. High concentration of toxic metal ions is above permissible limits in Nairobi industrial area (Kinuthia et al. 2020). The levels of Pb in the river, stream and spring water samples in certain sites in Turkey were somewhat higher than the Pb values reported in the literature for natural waters (Kacmaz 2020). Furthermore,

Zhou et al. (2020) have surveyed total concentrations and sources of heavy metal pollution in global river and lake water bodies from 1972 to 2017. They concluded that over the years, metal ion contamination is increased in rivers and other water bodies.

A recent report by United Nations concluded that "water quality will be adversely affected by increase in temperatures due to climate change, which will reduce dissolved oxygen in water. Hence, in coming times water's self-purifying capability will be reduced. Much of the impacts of climate change will be observed in tropical zones where most of the developing world is located" (UN-Water 2020). Developing world has less resources to tackle the climate change impacts including water purification. It is not possible for developing nations to establish big infrastructure to provide clean drinking water to population to their households. Point-of-use water filters for households are common in developing countries. The adsorptive removal of contaminants from portable water is an effective method than the others for removal of contaminants due to its simplicity in design,

application and regeneration of adsorbents (Gupta and Suhas 2009; Yi et al. 2012; Vieira et al. 2014). Activated carbon, which is obtained from hard wood (high lignin) using slow pyrolysis process (pyrochar), is commonly employed in commercial water filters. Activated carbon prepared from biomass (biochar/ hydrochar) is an alternate and has good adsorption capacity than the other adsorbents for removal of contaminants including metal ions (Zhang et al. 2019). Char produced from soft wood (low lignin) using hydrothermal process has advantage of being produced at low temperature and without preliminary drying step unlike pyrolytic process. Waste biomass from food source being a renewable raw material can be used for carbon sequestration and major constituent for the preparation of hydrochar and activated carbon (Liu and Zhang 2009). Hydrochars produced from various biomasses and under variable conditions are intensively used in metal ion-contaminated soil remediation (He et al. 2019; Yuan et al. 2019). Furthermore, hydrochars have found applications in removal of metal ions from aqueous solutions as well (Inyang et al. 2016; Premarathna et al. 2019; Zhao et al. 2019). Mango peel contains carotenoids, polyphenols, hemicellulose, lipids, protein, cellulose and pectin (Ajila et al. 2007). Among these cellulose and pectin are the polysaccharide components present in peels. These polymers are rich in functional groups such as carboxylic hydroxyl (in cellulose) and galacturonic acids (in pectin). These strongly bind metal cations in aqueous solution (Iqbal et al. 2009). Therefore, using mango peels waste to prepare activated hydrochar has the potential of use as adsorbent for the removal of toxic metals from aqueous solution. These studies have shown strong potential for hydrochars in water treatment; however, most of the studies suggest these materials for the treatment of wastewater.

The objective of this study was to explore the potential of hydrochars in drinking water treatment, specifically for application in point-of-use water filters. This study involves the hydrothermal conversion of food waste (mango peels) into hydrochar and investigates the suitability of developed material in fixed-bed continuous flow process for potential use in point-of-use candle-type water filters. Lead (Pb) was selected as model metal ion pollutant due to its universal contamination in aqueous systems and its toxicity. Many manufacturing industries utilize lead in the form of semiconductor, metal plating, manufacturing of battery and paint that may contribute to the pollution of the environment (Goel et al. 2005; Kumar and Bandyopadhyay 2006; Manasi et al. 2014). Furthermore, adsorption process in continuous flow is investigated through Bohart–Adams, Thomas and Yoon–Nelson models, and the developed system is applied to contaminated real water samples.

Materials and methods

Chemicals

The chemicals were used as received in these experiments without further purification. The solutions were prepared in deionized water. The complete name of chemical, formula, CAS number, supplier and its purity are presented in Table 1.

Collection of real water samples

Total five groundwater samples were collected from different areas of district Matiari, Sindh, Pakistan. The samples were collected from hand pumps and motor pumps mostly used for human consumption. Samples were preserved using HNO_3. Before analysis, water samples were filtered to remove suspended particles. Lead concentration was analyzed for each sample before and after adsorption.

Table 1 List of chemical compounds with CAS registry number, supplier and purity

Chemical name	Chemical formula	CAS number	Supplier	Sample purity
Lead nitrate	$Pb(NO_3)_2$	10099-74-8	Merck	99%
Sodium chloride	NaCl	7647-14-5	Daejung	> 99.9%
Sodium hydroxide	NaOH	1310-73-2	Sigma-Aldrich	99–100.5%
Hydrochloric acid	HCl	7647-01-0	Sigma-Aldrich	35.0–37.0%
Methylene blue	$C_{16}H_{18}N_3SCl.3H_2O$	61-73-4	Sigma-Aldrich	99%
Iodine	I_2	7553-56-2	Sigma-Aldrich	99%
Sodium thiosulfate	$Na_2S_2O_3.5H_2O$	10102-17-7	Sigma-Aldrich	99–101%
Potassium iodide	KI	7681-11-0	Sigma-Aldrich	99%
Calcium chloride	$CaCl_2$	7440-70-2	Merck	99–103%
Magnesium chloride	$MgCl_2$	7786-30-3	Sigma-Aldrich	99%
Starch	$(C_6H_{10}O_5)_n$	9005-84-9	Merck	99%
Phenolphthalein	$C_{20}H_{11}O_4$	77-09-08	Sigma-Aldrich	98–102%

Material for activated hydrochar preparation

Collected biomass

Different biomasses are used as adsorbent for the removal of toxic metals. Amongst mango peels are preferred a simple, natural and cheap adsorbent for the metal removal from aqueous solution (Gebretsadik et al. 2020). Sindhri mango peels were selected because large quantities are wasted during peak seasons. There are varieties of mangoes in Pakistan with a distinctive shape, taste and size. Sindhri is a leading variety of mango cultivated in Sindhri town, Mirpurkhas district, Sindh, Province of Pakistan. Sindhri mangoes bit tangy early in the season. Fresh mango peels were collected from different fruit juice shops of Sindh, Pakistan. The peels were then finely chopped and kept frozen at − 18 °C till used. The powdered material sieved and particle size 0.8–1.0 mm was used for metal adsorption studies.

Preparation and activation of hydrochar

Hydrochar was produced by hydrothermal treatment, using a method described in the following section (Titirici 2012). In synthesis, 15.0 g of fresh mango peels was added into different 25 mL of Teflon-lined stainless-steel autoclaves. Samples were heated in electric oven at 200 °C for five hours to obtain carbon-enriched product called hydrochar. The solid carbon product (hydrochar) was washed continuously with distilled water to obtain neutral pH carbon product. The sample was then dried at room temperature. Activated hydrochar (ACH) was prepared from hydrochar by taking 100 g of solid hydrochar in a porcelain evaporating dish and heated to 400 °C, 600 °C and 800 °C separately for one hour in a muffle furnace, under N_2 atmosphere with flowing rate of 180 mL/min to obtain various activated hydrochars. Activated hydrochars were cooled in the furnace overnight under N_2 atmosphere with flow rate of 60 mL/min. Products were coded as ACH 400, ACH 600 and ACH 800. Activated hydrochar yields were calculated according to the given equation:

$$Yield\ of\ AC\ (wt\%) = \frac{Weight\ of\ activated\ carbon}{Weight\ of\ hydrochar} \times 100 \quad (1)$$

Preparation of lead(II) standards

A stock of 1000 mg/L lead solution was prepared by dissolving appropriate amount of lead nitrate in distilled water. Further desired lead solutions were prepared from stock solution by diluting with distilled water.

Analysis of lead(II) ions

The residual and real concentrations of lead for optimization and column studies were analyzed by Flame Atomic Absorption Spectrometer (PerkinElmer AAnalyst 800, Singapore) that was equipped with hollow cathode lamp source, burner and air acetylene flame. For the analysis of breakthrough curve, effects of adsorbent bed heights (1.3, 2.4 and 4.4 cm), flow rates (6, 9 and 12 mL/min) and sorbate concentrations (60, 80 and 100 mg/L) were evaluated. For real samples, initial and residual concentrations of lead were determined using inductively coupled plasma optical emission spectroscopy (ICP-OES Thermo iCAP 7000, Germany); because of better sensitivity of ICP-OES, the real samples were analyzed at a lower concentration.

Characterization of activated hydrochar

The physicochemical characterization of activated hydrochars (ACH 400, ACH 600 and ACH 800) was studied for their structure and compositions determination before and after adsorption process. Moisture content was determined according to the ASTM (2016) method D 2867. Moisture content of activated hydrochars was measured by difference in weight after drying at 110 °C. For the determination of moisture, a 15 g of each material was added in crucibles and covered with its lid. The crucibles were preheated in oven with temperature of 110 °C for one hour; after that, crucible was cooled in a desiccator and weighed. Moisture (%) was calculated by taking the difference in weights before and after drying in an oven. The pH was also determined by using the procedure mentioned in ASTM (2016) D 3838. A 3.0 g of sample was soaked in 300 mL of deionized water for 30 min with occasional stirring. The pH of aqueous phase was then measured using portable pH meter.

Total acid density of activated hydrochars was calculated by the acid–base back titration method. Acidic groups including carboxylic, phenolic and sulfonic groups were involved in the acid density measurement. For acid density measurement, 0.05 g of material added in 50-mL conical flask and was added 15 mL of 2 M sodium chloride solution. The solution was sonicated for about 30 min and then filtered. The filtrate solution was titrated against 0.02 M sodium hydroxide by using phenolphthalein as an indicator(Mo et al. 2008).

Total acid density of activated hydrochars is calculated by the given equation:

$$C(H) = C(OH) * \Delta V/m \tag{2}$$

where V is volume of titrant in mL, m is the mass of substance in g and OH designates the molar concentration of sodium hydroxide.

Methylene blue (MB) number is defined as the milligrams amount of methylene blue adsorbed per gram of carbon. Langmuir isotherm adsorption study was conducted for methylene blue number estimation. The stock solution of methylene blue (1000 mg/L) was prepared and solution further diluted to five different concentrations (Hameed et al. 2007). A 30 mg of each activated hydrochar was added into five different 250-mL Erlenmeyer flasks. A 20 mL of each methylene blue solution was added into flasks and placed in a thermal shaker with 150 rpm at room temperature (28 ± 2 °C) for a time period of 4 h. The methylene blue concentration determined by carrying out measurements in double-beam UV–Vis spectrophotometer at wavelength 665 nm (Rajamani et al. 2018). Adsorbed amount of methylene blue number at equilibrium q_e (mg/g) is calculated by using equation:

$$qe = \frac{(Co - Ce).V}{M} \tag{3}$$

where C_0 is initial and Ce represents equilibrium concentration of methylene blue solution, while M is the mass in g of sorbent and V is volume in mL of treated solution. Langmuir linear model was applied to evaluate the maximum adsorbed amount of methylene blue by each sample calculated by equation:

$$\frac{Ce}{qe} = \frac{1}{Qob} + \frac{Ce}{Qo} \tag{4}$$

where qe is the amount adsorbed at equilibrium in mg/g, Ce is the initial concentration, Q_0 is maximum sorption capacity and b represents Langmuir equilibrium constant in mL/mg. The values of Q_0 and b were determined graphically. A plot of Ce/qe versus Ce gives a straight line of slope $1/Q_0$, which corresponds to complete monolayer coverage (mg/g), and the intercept is $1/Q_0b$.

Iodine number was determined by method D 4607 mentioned in ASTM (2016). The iodine adsorbed in milligrams by one gram of carbon is known as iodine number. The quality of activated hydrochar was expressed in terms of iodine number range from 500 to 1200 mg/g. For the determination of iodine number, 10 mg of each activated hydrochar was kept in contact with 10 mL of a 0.01 N iodine solution after treating with 1 mL of 5% HCl. The solution was stirred for 30 s and then filtered. After filtration, 5 mL of filtrate solution was titrated against 0.1 N sodium thiosulfate by adding few drops of starch as an indicator to evaluate the remaining concentration of iodine.

The amount of activated hydrochar for each sample to be used in the determination of iodine number is governed by the activity of the carbon. The iodine amount is adsorbed in milligrams by one gram of carbon. The iodine number is the X/M value when the iodine residual concentration must be 0.01 N. Iodine number is calculated by the given equation:

$$X/M = \{(N_I \times 126.93 \times V_I) - [(V_I + V_{HCl})/V_F] \times (N_{Na2S2O3} \times 126.93) \times V_{Na2S2O3}\}/M_c \tag{5}$$

where N_I is the normality of iodine solution, V_I is the volume in mL of iodine solution, V_{HCl} is the added volume of 5% HCl, V_F is the filtrate volume used in titration, $N_{Na2S2O3}$ is the normality of sodium thiosulfate, $V_{Na2S2O3}$ is the consumed volume of sodium thiosulfate solution and M_C is the mass in g of activated hydrochar.

Fourier transform infrared (FTIR) spectroscopy (Thermo Nicolet TM iS10, ThermoScientific, USA) equipped with diamond crystal was used to find functional groups present on the surface of activated hydrochar in the wavenumber range of 500–4000 cm^{-1}. A small amount of ground powdered sample was placed on ATR crystal to record the FTIR spectra in single bounce attended total reflectance mode.

Scanning electron microscope (SEM) (JSM-6491 LV, Joel. Japan) was employed for surface morphology of activated hydrochars. Twenty milligrams of sample was dispersed in 30 mL of water and dry overnight in oven at 60 C and were characterized from the laboratory of Metallurgy department Mehran University of Engineering and Technology Jamshoro, Sindh, Pakistan.

The surface area, pore size and pore volume were examined by Brunauer, Emmett and Teller (BET) multipoint technique (Autosorb-1, Quantachrome, AsiQwin, USA) using nitrogen adsorption at 78 K. Before analysis of material, the degassing temperature was set at 180 °C for six hours.

Selection of prepared activated hydrochar

The removal percent of lead(II) ions at breakthrough point (R_b, %) was calculated by passing a 100 μg/mL standard aqueous solution of lead in the column through ACH 400, ACH 600 and ACH 800. The effluent concentration of lead (C_f) was evaluated by flame atomic absorption spectroscopy (FAAS). The sorbent with high removal efficiency was selected for further study. The metal removal efficiency of metal at breakthrough point for each is calculated using equation:

$$Removal\ efficiency\,(\%) = \left[1 - \left(C_f/C_i\right)\right] \times 100 \qquad (6)$$

where C_i is the initial and C_f represents residual concentration of lead.

Column setup and experimental procedure

Fixed-bed column sorption experiment was used to measure dynamic behavior for the removal of lead. The borosilicate glass column with 1 cm internal diameter and 30 cm length was used for experiment. The column was functioned with down-flow liquid mode. A known weight of biosorbent was packed into a column between supporting layers of glass wool amount. As the study focuses on the removal of lead from real water samples, hence the pH study was not conducted, and neutral pH was considered throughout the study. The continuous flow experiment was performed at given room temperature 28 ± 2 °C. The lead working solutions were pumped using a Gilson MINIPULS® 3 Peristaltic Pump. Lead effluent solution was collected at various time intervals (up to 100 min) for examination of break point and exhaustion point in the shape of breakthrough curve. The experiments were continued until column become saturated and obtained a constant lead concentration. The effluent concentration of lead was analyzed in flame atomic absorption spectroscopy. For the analysis of breakthrough curve, effects of adsorbent bed heights (1.3, 2.4 and 4.4 cm), flow rates (6, 9 and 12 mL/min) and sorbate concentrations (60, 80 and 100 mg/L) were evaluated. The experimental adsorption results were also fitted by kinetics mathematical models Adams–Bohart, Thomas and Yoon–Nelson.

Fixed-bed column data analysis

Column data analysis was evaluated through the breakthrough curve data (breakthrough & exhaustion points) in a continuous fixed-bed system. Breakthrough time/break point (t_b) is the time required for approaching a specific breakthrough concentration usually 10% ($C_t/C_0 = 0.1$) of the influent concentration, whereas exhaustion/saturation time is the time where effluent concentration (C_t) influences 90% ($C_t/C_0 = 0.9$) of the influent concentration. The S-shaped breakthrough curve obtained by C_{eff}/C_o against interaction time (min) (Kumar and Bandyopadhyay 2006).

Total adsorbed lead quantity (q_{total}) in mg was calculated with specified flow rate (Q), and lead concentration is equal to the area under the integrated plot of adsorbed concentration C_{ads} ($C_{ads} = C_0 - C_t$) (Hasan et al. 2010). It is calculated by the given equation:

$$q_{total} = \frac{QA}{1000} = \frac{Q}{1000} \int_{t=0}^{t=t_{total}} (Co - Ct)dt \qquad (7)$$

where A is the area of breakthrough curve, Q represents the flow rate in mL/min of the column and t_{total} shows total used flow time.

Total amount of lead (m_{total}; mg) in the column is calculated by the given equation:

$$m_{total} = \frac{Co \cdot Q \cdot t_{total}}{1000} \qquad (8)$$

Total removal of lead ions (%) is the ratio of total adsorbed lead amount to the total amount of lead ions calculated from given Eq:

$$Total\ removal\ of\ lead\,(II)\ ions\,(\%) = \frac{q_{total}}{m_{total}} \times 100 \qquad (9)$$

The equilibrium uptake capacity (q_{eq}) in mg/g of lead is the adsorbed amount of lead per unit weight of adsorbent, which was determined from equation:

$$q_{eq} = \frac{q_{total}}{m} \qquad (10)$$

where m represents mass of sorbent (g) used in the column.

Modeling for fixed-bed column

Adam–Bohart model

Adam–Bohart model is related to the surface reaction theory. It describes the proportionality between the rate of adsorption and residual capacity of sorbent and sorbate concentration (Bohart and Adams 1920). This model was selected for the account of initial part of the breakthrough curve data (breakpoint)(Sarin et al. 2006; Saadi et al. 2013). It is expressed as in Eq:

$$In\left(\frac{C_t}{C_o}\right) = K_{AB}C_o t - K AB \cdot No\left(\frac{Z}{U_o}\right) \qquad (11)$$

where k_{AB} is the Adam–Bohart constant (L/mg min), N_0 represents the maximum saturation concentration (mg/L) or maximum ion adsorption capacity per unit volume of adsorbent column and Z is the bed depth of the column (cm). Uo is the linear flow velocity in cm/min measured by calculating volumetric flow rate over the bed cross-sectional area. k_{AB} and No values are calculated by plotting of ln (Ct/Co) against time (minute).

Thomas model

This model describes breakthrough curves data and influence of biosorption process of the column system (Thomas 1944). It obeys the second-order kinetic reaction with insignificant axial dispersal in the column adsorption process. Thomas model also assumes that biosorption occurs by mass transfer at the interface (Apiratikul and Pavasant 2008). It is expressed as in Eq:

$$ln\left[\frac{C_o}{C_t} - 1\right] = \frac{k_{Th}q_o m}{Q} - k_{Th}C_o t \tag{12}$$

where q_o represents the maximum solid phase lead concentration per weight of adsorbent (mg/g). k_{Th} is the Thomas rate constant (mL/min mg). q_o and k_{Th} values are calculated by plotting of ln $[(C_o/C_t) - 1]$ against time (minute).

Yoon–Nelson model

This model defines adsorption process and breakthrough adsorbate probability. It assumes that the rate of adsorption decreases when the probability of adsorbate is proportional to the probability of adsorbate breakthrough on the adsorbent(Yoon & Nelson 1984). Yoon–Nelson model is expressed in Eq:

$$In\left(\frac{C_t}{C_o - C_t}\right) = k_{YN}.t - \tau.k_{YN} \tag{13}$$

where k_{YN} represents Yoon–Nelson proportionality constant (min^{-1}). The τ is the time required for 50% adsorbate breakthrough in minutes. k_{YN} and τ values calculated by plot of ln $(C_t/(C_o–C_t))$ versus time (minute).

Results and discussion

Characterization

Physicochemical characteristics of the activated hydrochars

A 15.0 g of wet mango peels produced 2.0 of hydrochar, which shows that biowaste can be successfully converted into hydrochar with conversion efficiency of 13.33%. However, hydrochars cannot be directly used for the treatment of drinking water in fixed-bed packing columns. Hydrochars leach yellow color when in contact with water and has tendency to stick together under mild pressure and therefore clogs the column. Leachate from hydrochars may be considered as oligomers of phenols (Boucard et al. 2020), which are unreacted and trapped-in components in hydrochar. Therefore, hydrochars are thermally treated at various temperatures to make them suitable for drinking water applications.

Table 2 shows the yield of thermally activated hydrochar from hydrochar produced using hydrothermal carbonization process. The % yield for ACH 400, ACH 600 and ACH 800 was found to be 44.63%, 38.36% and 26.12%, respectively. The % yields of activated hydrochars decrease with increasing temperature because during activation colloidal and low-density carbon in hydrochar evaporate and get converted into soot.

Commercially available activated carbons are tested using ASTM standards with certain physicochemical characteristics like moisture content, contact pH, iodine number and methylene blue number when employed in water treatment. Therefore, activated hydrochar produced by thermal treatments of hydrochars was also tested for same characteristics. The results of physicochemical characteristics for activated hydrochars obtained at various temperatures are given in Table 3. The contact pH of the ACH 400, ACH 600 and ACH 800 was found to be 6.5, 6.77 and 6.81, respectively, which is close to neutral as compared to pyrolytic activated carbons, which is basic in nature (Zewail and Yousef 2015). Moisture (%) of activated hydrochars was 5.08, 10.05 and 4.04, respectively, which were found

Table 3 Physicochemical characteristics of the activated hydrochars

Parameters	Value		
	ACH 400	ACH 600	ACH 800
pH	6.5	6.77	6.81
Moisture (%)	5.08	10.05	4.04
Acid density (mmol g^{-1})	0.1	0.08	–
Methylene blue number (mg/g)	909.09	526.31	714.28
Iodine number (mg/g)	869.01	1179.81	915.93
Surface area (m^2/g)	3.711	6.610	6.174
Pore volume (c.c./g)	0.009	0.016	0.010
Pore diameter (nm)	6.282	4.736	3.819

Table 2 Conversion efficiency of hydrochar to activated hydrochars at various temperatures

Sample Id	Activation temp (°C)	Weight before activation (g)	Weight after heating (g)	Yield (%)	Std ($\pm$) (n=3)
ACH 400	400	19.76	9.21	44.63	2.82
ACH 600	600	15.32	6.25	38.36	3.48
ACH 800	800	19.82	5.03	26.12	1.01

within the specified range (3–10% max) recommended by ASTM (2016) and shows that activated hydrochars quality is good enough and preferable for adsorption processes for the treatment of liquid effluents to be used in the column. The higher moisture content for ACH 600 may be due to enhanced pore volume as compared to AC 400, which reflects its capacity to hold more water in its pores. The iodine number for the ACH 400, ACH 600 and ACH 800 was to be 869.0, 1179.81 and 915.93 mg/g. Iodine number is measure of double bonds; here, it shows that ACH 600 has more double bonds than other materials. The methylene blue number of activated hydrochars was found to be 909.09, 526.31 and 714.28 mg/g, respectively. Methylene blue number indicates the color removal efficiency of activated carbon. Methylene blue is a positively charged dye, which interacts with adsorbent through surface charge and pores in it. MB number in Table 3 shows that ACH 600 has less negatively charged centers as compared to ACH 400. The obtained results indicate good adsorption capacity of the materials prepared from waste biomass has micropore network formation and surface charges (Raman 2015; Rajamani et al. 2018).

Total acid density of activated hydrochars was measured using the back titration method, which is a measure of acidic functional groups on surface. Total acid density for ACH 400 and ACH 600 was 0.1 and 0.08 mmol/g, respectively, while zero value was found for ACH 800. Total acid density of activated hydrochars decreased from lower to zero because during pyrolysis of HTC in the absence of oxygen aromatization increases and CO_2 evolves due to decomposition of acidic oxygenated functional groups. Higher acid density imparts better cation-exchange-type capacity of material.

Morphology, porosity and surface functionalities

All three activated hydrochars obtained at various temperatures were amorphous in nature. X-ray diffraction pattern of ACH 400, ACH 600 and ACH 800 shows broad diffraction peaks at 2 $(\theta) = 23.100°$, 2 $(\theta) = 23.700°$ and 2 $(\theta) = 24.100°$ as shown in Fig. 1a–c. Two weak diffraction peaks at $2(\theta) = 43.100°$ and 2 $\theta) = 42.100°$ were also appeared for ACH 600 and ACH 800. The broad diffraction

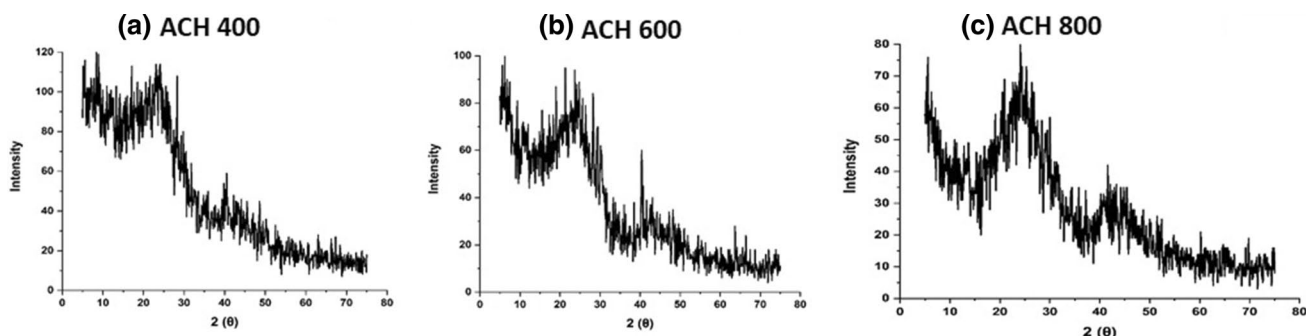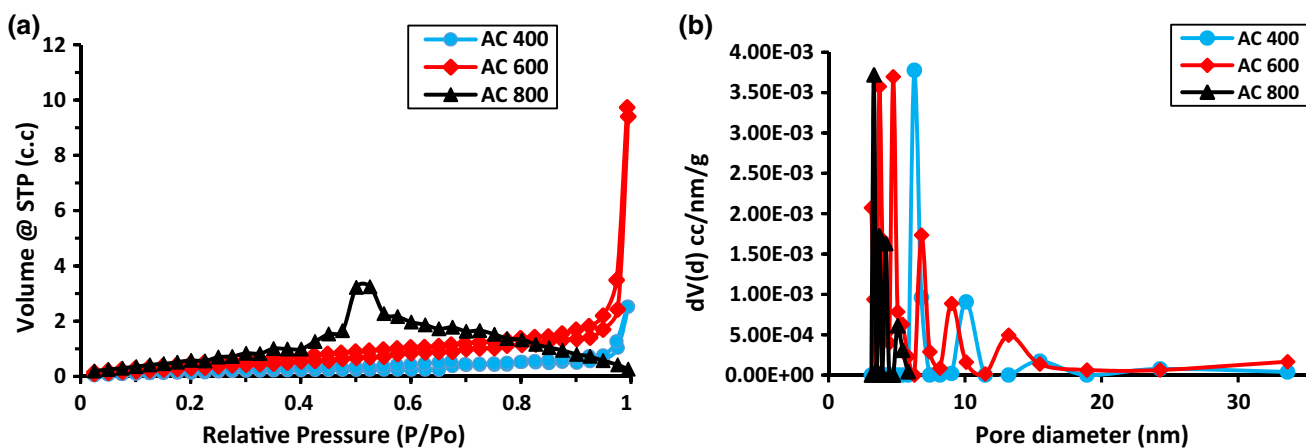**Fig. 1** XRD spectra of **a** ACH 400. **b** ACH 600. **c** ACH 800

Fig. 2 **a** N_2 adsorption–desorption isotherm. **b** Pore size distribution of ACH 400, ACH 600 and ACH 800

peaks confirm the amorphous structure amorphous nature of the activated hydrochars (Rao et al. 2011; Settle 1997).

The three activated hydrochars showed different pore sizes and volumes but similar porous structure. The nitrogen adsorption–desorption isotherm indicated type III IUPAC classification, which represents unrestricted multilayer formation and mesoporous structure for activated hydrochars (Tsubouchi et al. 2003) as given in Fig. 2a. H3 hysteresis loop type III isotherms indicated aggregates plate like particles with slit-like pores (Chen & Fang 2011). The surface area and pore volume for ACH 400, ACH 600 and ACH 800 were found to be 3.711 m^2/g, 6.610 m^2/g, 6.174 m^2/g and 0.009 c.c/g, 0.016 c.c/g, 0.010 c.c/g. A very negligible pore volume and low surface area are common for thermally activated hydrochar. The BJH method was used to obtain the average pore diameter of activated hydrochars. The narrow distribution curves with size less than 20 nm confirm the mesoporous structure of activated hydrochars as indicated in Fig. 2b. BET surface area, pore volume and pore size results are also mentioned in Table 3.

SEM images of activated hydrochars are shown in Fig. 3. From the images, it is observed that particles sizes and shapes of the activated hydrochars are in wide range. Figure 3a represents ACH 400, which shows wider particle size distribution, but in Fig. 3b [ACH 600] particle seems condensed and interconnected while in Fig. 3c [ACH 800], particles with some globular agglomerated are seen. These morphological changes can be attributed with the increase in activation temperature.

Fourier transform infrared (FTIR) spectroscopy was employed for identification of functional groups present on the surface of activated hydrochars (Fig. 4a–c. The peak observed at 1590 cm^{-1} was assigned to stretching vibration of C=C alkene group, which disappears in ACH 600 and ACH 800. The peak is at 1120 cm^{-1} due to C–O in hydroxyl group (–C–O–H) from the carbohydrate. The peaks are at 1051, 880 and 873 cm^{-1} due to C-H in-plane and out-of-plane vibration. Thus FTIR spectra indicated that the certain oxygenated functional groups (OFG) such as ether, phenolic, carbonyl, hydroxyl and carboxyl groups present on the surface of activated hydrochars (Liu et al. 2010). The hydroxyl group diminishes continuously, and aromatization increases with increase in activation temperature.
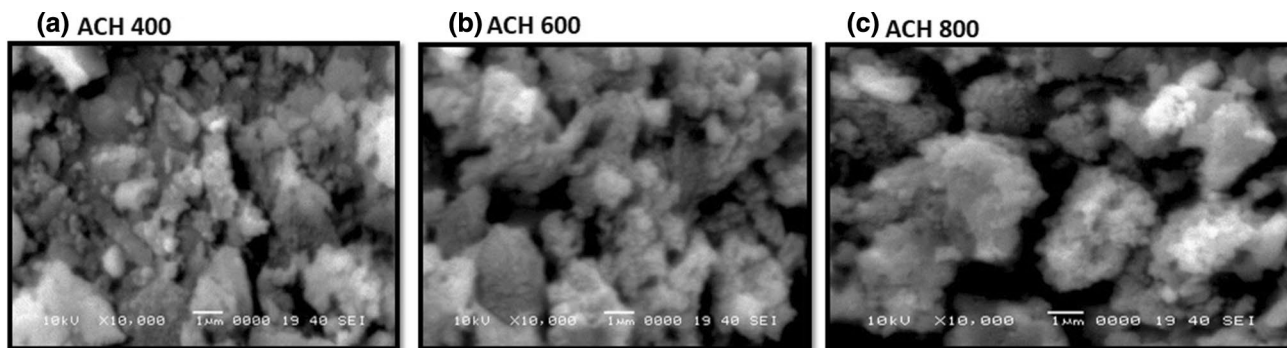

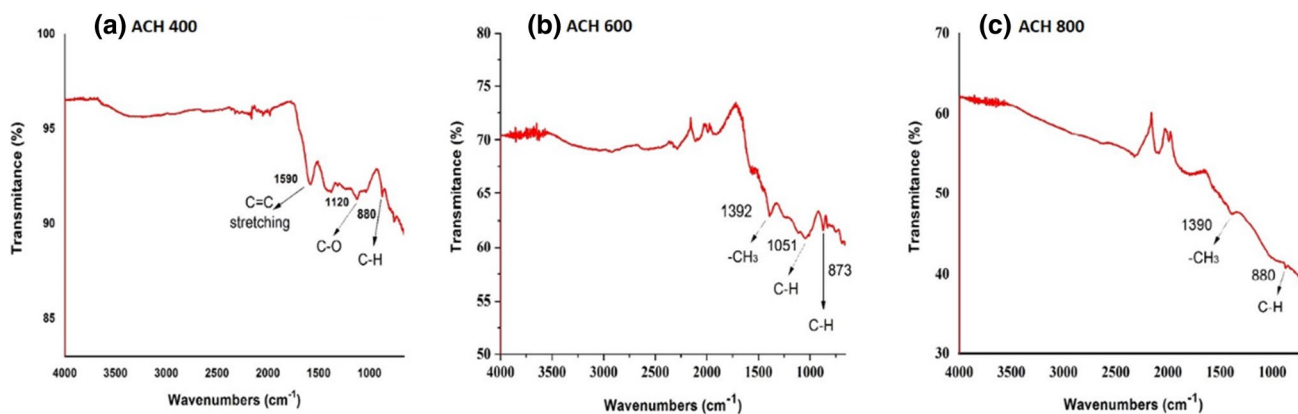**Fig. 3** SEM images of activated hydrochars **a** ACH 400, **b** ACH 600 and **c** ACH 800

**Fig. 4** FTIR spectra of **a** ACH 400, **b** ACH 600 and **c** ACH 800

Table 4 Fixed-bed column parameters of lead(II) ions biosorption by ACH 400

Bed height Z (cm)	Co (mg/L)	Flow rate (mL/min)	Breakthrough time t_B (min)	Adsorption capacity (mg/g) (RSD n = 3)	Total removal (%)
1.3	100	12	10	35.08 ± 1.02	87.67
2.4	100	12	18	38.31 ± 3.11	88.70
4.4	100	12	25	26.67 ± 2.65	88.90
2.4	100	6	30	28.99 ± 0.76	80.56
2.4	100	9	25	39.83 ± 3.45	88.49
2.4	100	12	18	38.31 ± 2.41	88.70
2.4	60	12	30	38.63 ± 4.76	89.39
2.4	80	12	20	34.03 ± 1.11	88.59
2.4	100	12	18	38.31 ± 2.65	88.70
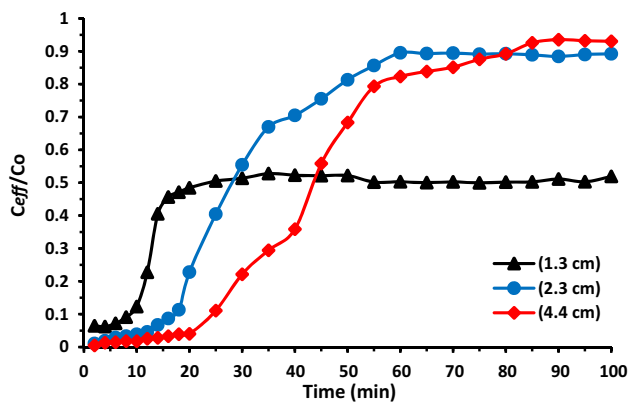
Fig. 5 Effect of bed heights on breakthrough curve (flow rate 12 mL/min, Conc. 100 mg/L)
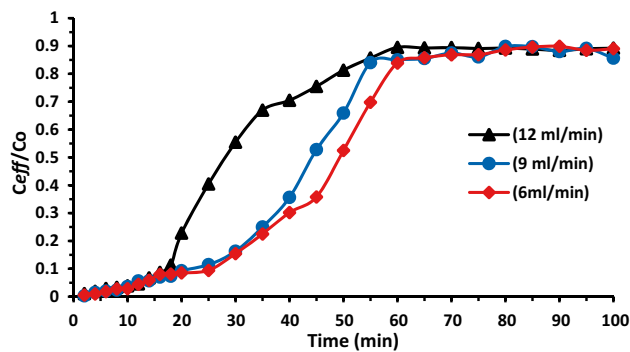
Fig. 6 Effect of flow rates on breakthrough curve (bed height 2.4 cm, Conc. 100 mg/L)

Evaluation of dynamic lead removal efficiency

Effect of activation temperature on lead removal

Column adsorption study was used for removal of toxic element lead using materials ACH 400, ACH 600 and ACH 800. Optimized parameters of bed depth (2.4 cm), influent flow rate (12 mL/min) and initial lead concentration (100 mg/L) were used for different activated hydrochars. The maximum removal efficiency for ACH 400, ACH 600 and ACH 800 was 99.43%, 93.07% and 92.22%. *This indicates that ACH 400 is a better sorbent compared to others for lead removal and was selected for further adsorption study.* Column adsorption process for breakthrough curves data with adsorbent bed heights (1.3, 2.4 and 4.4 cm), inlet feed flow rates (6, 9 and 12 mL/min) and sorbate concentrations (60, 80 and 100 mg/L) was evaluated. The results at breakthrough times (t_B) are presented in Table 4.

Effect of bed heights

Column data analysis was evaluated through the breakthrough curve data breakthrough point (usually 10% (C_t/$C_0 = 0.1$) of the influent concentration) and exhaustion point (effluent concentration influences 90% (C_t/$C_0 = 0.9$) of the influent concentration) in a continuous fixed-bed system. Breakthrough curves of lead (II) ions use different bed heights 1.3 (0.3 g), 2.4 (0.5 g) and 4.4 cm (1 g) with 12 mL/min influent flow rate and 100 mg/L of initial lead concentration (Fig. 5). The breakthrough time (t_B) increased with increasing bed height. 10% breakthrough time was found to be at 10, 18, and 25 min for bed heights 1.3, 2.4 and 4.4 cm, respectively. This is due to large specific surface of the sorbent and more binding sites available for sorption process.

The more wastewater volume treated for longer bed height with maximum removal percentage of metal ions, while for reduced bed height gets saturated earlier with lesser breakthrough time. The lead (II) ions did not diffuse into the whole of the sorbent mass (Lodeiro et al. 2006). The adsorption capacities for 1.3, 2.4 and 4.4 cm were found to

be 35.08, 38.31 and 26.67 mg/g (Table 4). The equilibrium uptake capacity 38.31 mg/g was calculated for 2.4 cm bed height and selected further as the optimum bed height for different experiments.

Effect of flow rates

The different flow rates (6, 9 and 12 mL/min) were studied with bed height of 2.4 cm and lead concentration of 100 mg/L. The decreases of flow rate cause increase in breakthrough time (t_B) with constant bed height and lead concentration (Fig. 6). The 10% breakthrough time was 30 min, 25 min and 18 min for 6, 9 and 12 mL/min flow rates, respectively. At higher flow rate, contact time of lead solution decreases and lead solution has lesser contact with sorbent to diffuses into pores. Amount of lead ions were adsorbed and had weak distribution of the solution into the column, whereas at lower flow residence time of lead solution that is larger allows to diffuse and attain active sites of sorbent (Goel et al. 2005). Equilibrium adsorption capacities of lead (II) ions were 28.99, 39.83, 38.31 mg/g with flow rate of 6, 9 and 12 mL/min, respectively, as mentioned in Table 4. Adsorption capacities increased with increasing flow rate which may be due to faster adsorption kinetics that simulates the quick adsorption of lead ions and pave the way for quick saturation of sorption sites. Therefore, at higher flow rates breakthrough time reaches fast and results in higher adsorption capacity.

Effect of concentrations

The effect of different lead concentrations (60, 80 and 100 mg/L) was studied on its breakthrough curves performance with constant bed height of 2.4 cm and influent flow rate of 12 mL/min. Ten percentage breakthrough time was found to be 35 min, 25 min and 18 min for concentrations
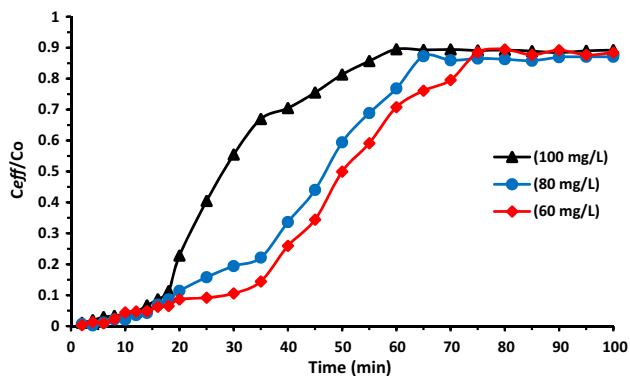
Table 5 Comparison of adsorption capacities of lead to other adsorbents

Adsorbent	Adsorption capacity (mg/g)
Green coconut shells (Sultan et al. 2020a)	54.62
Allspice (Sultan et al. 2020b)	16.2
Granular activated carbon (FAOSTAT 2005)	2.013
Bentonite (Ajila et al. 2007)	15.38
Bituminous coal (Iqbal et al. 2009)	8.89
Sphagnum moss peat (Gebretsadik et al. 2020)	19.90
Banana peel (Abu-El-Halawa and Zabin 2017)	2.18
ACH 400 (Current work)	38.31

of 60, 80 and 100 mg/L (Fig. 7). With the increase in lead concentration, the breakthrough time occurred earlier, and sorbent gets saturated early due to accessibility of binding sites. On the other hand, with the decrease in lead concentration, treated outlet volume was found higher, which leads higher breakthrough and exhaustion time (Aksu and Gönen 2004). The adsorption capacity of 60, 80 and 100 mg/L concentrations was found to be 38.63, 34.03 and 38.31 mg/g, respectively (Table 4).

Comparison study

Comparison of adsorption capacity with reported activated carbons

Lead adsorption capacity of thermally activated carbon obtained from hydrochar (ACH 400) was compared with reported activated carbons described in the literature for removal of lead and are mentioned in Table 5. Lead sorption efficiency is found superior to other activated carbons reported in the literature.

Comparison with other technologies used for lead removal

There are different types of techniques used for the removal of lead from contaminated water as mentioned in Table 6. These techniques have good removal efficiencies for lead, but has critical disadvantages which are related to long time process, non-selective, ineffective in removal of metal at low concentration and their significant expenses. Among all the methods, fixed-bed column adsorption study using activated hydrochar is one of the efficient methods for removal of contaminates from water. In comparison with other technologies, fixed-bed column adsorption study has many advantages such as low operating cost, simplicity, eco-friendly, high metal binding efficiency and good removal efficiency (Table 7).

Fig. 7 Effect of concentrations on breakthrough curve (bed height 2.4 cm, flow rate 12 mL/min)

Table 6 Comparison of removal efficiency of lead to other technology

S #	Mode of removal of lead	Method	Removal of lead (%)
1	Chemical precipitation (Abu-El-Halawa and Zabin 2017)	Lime and limestones	51.18
2	Ion exchange (Zewail and Yousef 2015)	synthetic (AMBERJET 1200 Na, zeolites and resins)	99
3	Membrane filtrations Ultrafiltration (Saffaj et al. 2004), Reverse osmosis (Algureiri and Abdulmajeed 2016), Nanofiltration (Al-Rashdi et al. 2011), Electrodialysis (Gurreri et al. 2020)	Membrane separation technique	92 97.5 84 90
4	Electrochemical method (Liu et al. 2013)	Redox reaction using Plexiglas cell	92.5
5	Coagulation–flocculation (Pang et al. 2011)	Use of aluminum sulfate, polyaluminum chloride (PAC) and magnesium chloride as coagulants	99
6	Remediation (Brooks et al. 2010)	isolation, immobilization, toxicity reduction, physical separation, Physicochemical, phytoremediation or Adam remediation	90
7	Adsorption (Long et al. 2014; Goel et al. 2005)	Batch and Fixed-bed column study	90–99
8	Adsorption (This work)	Fixed-bed column study	88.70

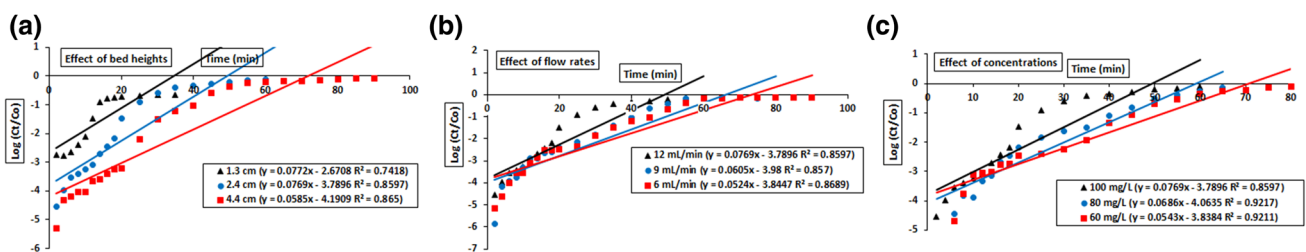**Table 7** Adam–Bohart model parameters for the sorption of lead ions by ACH 400

Bed height Z (cm)	Co (mg/L)	Flow rate (mL/min)	$K_{AB} \times 10^{-4}$ (L/min mg)	N_o (mg/L)	R^2
1.3	100	12	7.72	40,701	0.7418
2.4	100	12	7.69	30,799.74	0.8597
4.4	100	12	5.85	24,703.21	0.865
2.4	100	6	5.24	23,639.50	0.8689
2.4	100	9	6.05	30,326.25	0.857
2.4	100	12	7.69	31,799.74	0.8597
2.4	60	12	9.05	26,508.29	0.9211
2.4	80	12	8.57	29,617.35	0.9217
2.4	100	12	7.69	30,799.74	0.8597

Adsorption modeling of the breakthrough curve

The obtained data from the experiments were used in adsorption models to evaluate the relationship of the fixed-bed column parameters.

Adam–Bohart model

This model describes the initial part of the breakthrough curves for lead biosorption. It also helps in the prediction of column performance parameters of Adam–Bohart rate constant (k_{AB}) and maximum saturation concentration (N_o) with including of bed depths, flow rates and initial lead concentrations k_{AB} and no values calculated by plotting of ln (Ct/Co) against time (Fig. 8a–c). As shown in Table 6, maximum saturation concentration value (N_o) decreases with increasing bed depth due to more binding sites available for metal adsorption. Maximum saturation concentration value increased together with increase in both flow rates and initial concentrations. When initial lead concentration increases, adsorbent in the column become saturated. This condition is also for the increase in flow rates. Adsorbate volume was higher that causes the bed to saturate earlier with higher flow rate in the column (Goel et al. 2005). The regression coefficient values are found poor for this model; therefore, constants from this model carry no meaning and cannot be included in discussion (Saari et al. 2013).

Fig. 8 Adam–Bohart model curve for effects of **a** bed height, **b** flow rate and **c** concentrations
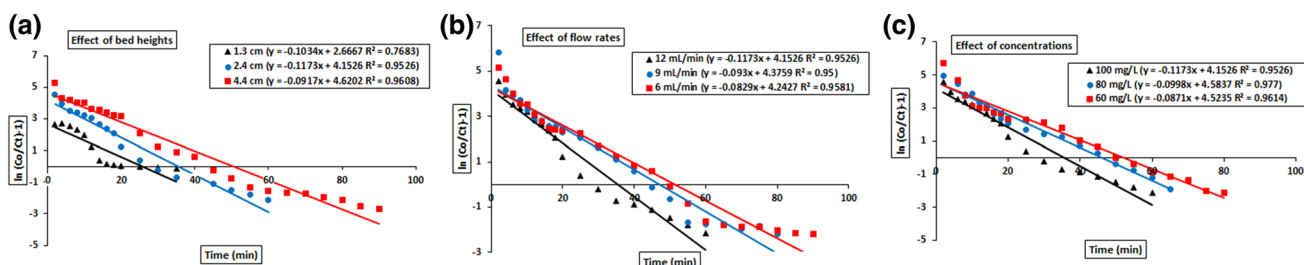
Fig. 9 Thomas model curve for effects of **a** bed height **b** flow rate and **c** concentrations

Table 8 Thomas model parameters for the sorption of lead ions by ACH 400

Bed height Z (cm)	Co (mg/L)	Flow rate (mL/min)	$K_{TH} \times 10^{-3}$ (mL/min mg)	q_o (mg/g)	R^2
1.3	100	12	1.03	103.16	0.7683
2.4	100	12	1.17	84.96	0.9526
4.4	100	12	0.92	60.46	0.9608
2.4	100	6	0.83	61.41	0.9581
2.4	100	9	0.93	84.69	0.95
2.4	100	12	1.17	84.96	0.9526
2.4	60	12	1.45	74.79	0.9614
2.4	80	12	1.25	88.18	0.977
2.4	100	12	1.17	84.96	0.9526

Thomas model

This model is mainly used for prediction of breakthrough curve data. The maximum solid phase concentration (q_o in mg/g) and Thomas kinetic coefficient (k_{TH}) describe the column behavior (Pilli et al. 2012). q_o and k_{Th} values were calculated by plotting of ln [($C_o/C_t) - 1$] against time (Fig. 9a–c). The increase in value of q_o decreases in bed height, while q_o value increases for both increase in initial concentration and flow rate as results mentioned in Table 8. This was because of high driving force for adsorption caused by high amount of lead perforated in the adsorbent and also difference of concentration between lead in the solution and with adsorbent (Zheng et al. 2016).

Yoon–Nelson model

The prediction of the breakthrough curves is the main objective of this model. This is simple theoretical model and considered for the single component and also predicted breakthrough time (Yahaya et al. 2011). k_{YN} and τ values were calculated by plot of ln ($C_t/(C_o – C_t)$) versus time as shown in Fig. 10a–c. The value of Yoon–Nelson constant (k_{YN}) is higher with increasing both flow rate and lead concentration, while value is smaller with increasing bed height. Higher rate of metal uptake for higher initial concentrations is due to the competition between adsorbate molecules for adsorption sites. The rate constant extent enhanced with increasing flow rate, while the τ (min)

Table 9 Yoon–Nelson model parameters for the sorption of lead by ACH 400

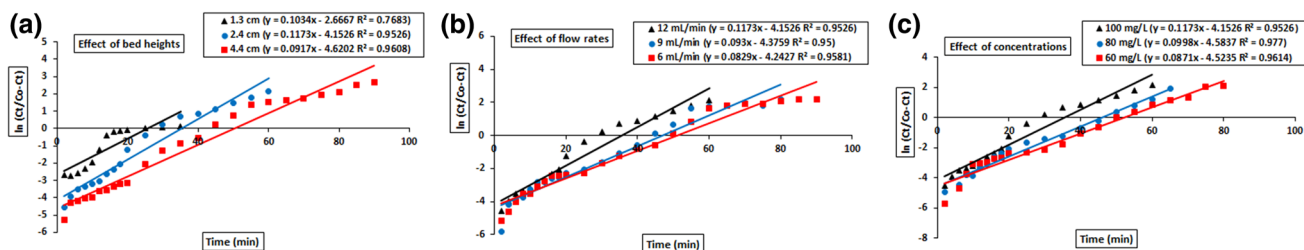| Bed height Z (cm)	Co (mg/L)	Flow rate (mL/min)	$K_{YN} \times 10^{-3}$ (min$^-$)	τ (min)	R^2
1.3	100	12	10.34	25.79	0.7683
2.4	100	12	6.51	35.40	0.9526
4.4	100	12	3.67	50.38	0.9608
2.4	100	6	2.76	51.18	0.9581
2.4	100	9	3.72	47.05	0.95
2.4	100	12	6.51	35.40	0.9526
2.4	60	12	2.90	51.93	0.9614
2.4	80	12	4.99	45.93	0.977
2.4	100	12	6.51	35.40	0.9526

Fig. 10 Yoon–Nelson model curve for effects of **a** bed height **b** flow rate and **c** concentrations

showed the reverse trend. Opposite behavior for both the rate constant and τ (min) increases bed height from 1.3 cm to 4.4 cm. (Table 9). Large value of k_{YN} at higher concentration causes to increase the force that may control mass transfer in the solution. Fifty percentage of breakthrough time (τ) increases with large bed height and decreases with increasing both flow rate and lead concentration because exhaustion period in the column occurs more rapidly. The longer time required for attaining exhaustion in the large bed height is due to the adsorbent providing more binding sites of lead ions (Calero et al. 2009).

The determination of the column parameters and breakthrough curves data was obtained by applying these three column models. Thomas and Yoon–Nelson provided a correlation with the prediction of breakthrough curves data with R^2 values of 0.95–0.977, which showed a good agreement between breakthrough curves and experimental data points. Adam–Bohart model equation was used to predict breakthrough times. The obtained results of this model at various influent concentrations showed good agreement with experimental data points with R^2 values (0.8597–0.9217). It was observed that R^2 values of Thomas and Yoon–Nelson were greater than the Adams–Bohart model. The Thomas and Yoon–Nelson models are well-fitted for lead adsorption experiment, which shows that the sorption of lead is reversible pseudo second order in nature without any axial dispersion. Also, sorption is instantaneous as it does not follow Adam–Bohart model, which is based on the theory that sorption is not spontaneous.

Interference study

Interference of calcium and magnesium on the removal of lead was evaluated by general column optimized procedure. A 1000 and 500 mg/L concentrations of calcium and magnesium ions were added individually to a solution that contains 100 mg/L of lead ions and passed into column with bed height 2.4 cm and flow rate 12 mL/min. The effluent concentration at breakthrough point was analyzed in flame atomic absorption spectroscopy.

Table 10 Interference of calcium and magnesium on the determination of lead in column

Metal	Added as	Amount in mg/L	Conc. After adsorption	Removal (%) (RSD n=3)
Lead	–	100	0.563	94.43 (0.5)
Calcium	CaCl$_2$	500	27.22	94.56 (1.9)
		1000	25.57	97.44 (1.4)
Magnesium	MgCl$_2$	500	1.798	99.64 (0.2)
		1000	0.184	99.98 (0.7)

Table 11 Removal (%) of lead from water samples after spiking lead amount

Matrix	Spiked amount of Pb^{2+} (mg/L)	Residual Conc. of Pb^{2+} (mg/L)	Removal (%) (RSD n=3)
Groundwater	40	0.283	99.29 (1.6)
	60	0.977	98.37 (1.2)
	100	0.389	99.61 (1.5)
Tap water	40	1.04	97.4 (1.7)
	60	6.09	89.85 (0.5)
	100	27.56	72.44 (1.9)
River water	40	0.512	98.72 (1.4)
	60	0.385	99.35 (1.1)
	100	0.451	99.54 1.7)

flame atomic absorption spectroscopy. The lead ions were still removed more than 90% from a solution with an error not exceeding 5% in the presence of calcium and magnesium ions as result shown in Table 10. No interference in the presence of high amounts of calcium and magnesium on the removal of lead ions was observed.

Applicability of activated hydrochar in treating water samples

Evaluation of real waters' matrix effect

Real water samples (groundwater, tap water, river water) were tested after spiking the different amounts of lead concentrations (40, 60 and 100 mg/L) through the packed bed column with bed height of 2.4 cm and flow rate of 12 mL/min. The effluent concentration at breakthrough point was analyzed in flame atomic absorption spectroscopy. More than 95% lead removed from groundwater, tape water and river water (Table 11).

Table 12 Removal (%) of lead from water samples after passing through ACH 400 in column

S #	Sample location	Initial Conc. of Pb^{2+} (mg/L)	Residual Conc. of Pb^{2+} (mg/L)	Removal (%) (RSD n=3)
1	Hala K.K CNG	0.045	0.0178	60.44 (0.2)
2	Bhitshah Bypass	0.0331	0.0107	67.67 (1.5)
3	Bhitshah city	0.0855	0.0247	71.11 (1.1)
4	Oderolal Village	0.0405	0.0157	61.23 (0.7)
5	Village Sher Muhammad Thora	0.0868	0.0184	78.80 (2.1)

Application to Real Water Samples

The present method is used to analyze lead ions in different water samples of district Matiari, Sindh. The concentration of lead in real water samples was analyzed before and after passing in the column by ICP-OES. A volume of 20 mL of each water sample was used for lead adsorption in fixed-bed column experiment with bed height of 2.4 cm and flow rate of 12 mL/min. The biosorbent has good capability to remove lead ions from contaminated water as results mentioned in Table 12. The lower percentage adsorption (60.44 to 78.80%) observed in real samples as compared to spiked samples prepared from pure distilled water may be due to the interference from some anions in the samples.

Conclusion

Hydrochars obtained from waste biomass using an environmentally safe hydrothermal carbonization process can be made useful for the treatment of water after activation at moderate temperature. Under this study, mango peels waste was converted to hydrochar with conversion efficiency of 13.33%. Mild activation temperature of 400 °C under nitrogen environment produced sufficiently porous and negatively charged carbonaceous materials, which can remove lead ions from aqueous solutions. ACH 400 can be packed in fixed-bed columns for continuous flow applications. The process can be adopted to produce activated hydrochars to replace activated carbon in areas where hardwood waste is not readily available. Activated hydrochar (ACH400) has acidic functional groups, which makes it a good cation exchanger with a carbon skeleton. Additionally, the faster and higher absorption efficiency of activated hydrochars makes it superior for use with a fixed-bed column continuous flow process. Column experiments on enriched and real water show that ACH 400 is also an excellent means of removing lead ions from the real water matrix at lower concentrations. The surface water parameters for the actual samples have been significantly improved, and the water quality parameters are close to the limits prescribed by the WHO after treatment with ACH 400. Thus, ACH 400 can be used as a suitable sorbent for a continuous flow system and can be applied on a large scale in water treatment applications. In the context of this study, the ACH 400 is an effective sorbent for the removal of lead compared to activated carbon (obtained from pyrolytic hardwood).

Declrations

References

Abu-El-Halawa R, Zabin SA (2017) Removal efficiency of Pb, Cd, Cu and Zn from polluted water using dithiocarbamate ligands. J Taibah Univ Sci 11(1):57–65. https://doi.org/10.1016/j.jtusci.2015.07.002

Ajila CM, Bhat SG, Prasada Rao UJS (2007) Valuable components of raw and ripe peels from two Indian mango varieties. Food Chem 102(4):1006–1011. https://doi.org/10.1016/j.foodchem.2006.06.036

Aksu Z, Gönen F (2004) Biosorption of phenol by immobilized activated sludge in a continuous packed bed: prediction of breakthrough curves. Process Biochem 39(5):599–613. https://doi.org/10.1016/S0032-9592(03)00132-8

Al-Rashdi B, Somerfield C, Hilal N (2011) Heavy metals removal using adsorption and nanofiltration techniques. Sep Purif Rev 40(3):209–259. https://doi.org/10.1080/15422119.2011.558165

Algureiri AH, Abdulmajeed YR (2016) Removal of heavy metals from industrial wastewater by using RO membrane. Iraqi J Chem Petrol Eng 17(4):125–136

Apiratikul R, Pavasant P (2008) Batch and column studies of biosorption of heavy metals by Caulerpa lentillifera. Biores Technol 99(8):2766–2777. https://doi.org/10.1016/j.biortech.2007.06.036

Bohart G, Adams E (1920) Some aspects of the behavior of charcoal with respect to chlorine. J Am Chem Soc 42(3):523–544

Boucard H, Weiss-Hortala E, Gueye F, Espitalier F, Barna R (2020) Insights in mechanisms of carbonaceous microparticles formation from black liquor hydrothermal conversion. J Supercr Fluids 161:104817. https://doi.org/10.1016/j.supflu.2020.104817

Brooks RM, Bahadory M, Tovia F, Rostami H (2010) Removal of lead from contaminated water. Int J Soil Sed Water 3(2):14

Calero M, Hernáinz F, Blázquez G, Tenorio G, Martín-Lara MA (2009) Study of Cr(III) biosorption in a fixed-bed column. J Hazard Mater 171(1):886–893. https://doi.org/10.1016/j.jhazmat.2009.06.082

Chen G, Fang B (2011) Preparation of solid acid catalyst from glucose–starch mixture for biodiesel production. Biores Technol 102(3):2635–2640. https://doi.org/10.1016/j.biortech.2010.10.099

FAOSTAT, F (2005) Statistical Database–Agriculture.

Frank A, Settle e (1997) Handbook of instrumental techniques for analytical chemistry. *Prentice Hall PTR*, 419.

Gebretsadik H, Gebrekidan A, Demlie L (2020) Removal of heavy metals from aqueous solutions using Eucalyptus Camaldulensis: an alternate low cost adsorbent. Cogent Chem 6:1. https://doi.org/10.1080/23312009.2020.1720892

Goel J, Kadirvelu K, Rajagopal C, Kumar GV (2005) Removal of lead(II) by adsorption using treated granular activated carbon: Batch and column studies. J Hazard Mater 125(1):211–220. https://doi.org/10.1016/j.jhazmat.2005.05.032

Gupta VK, Suhas, (2009) Application of low-cost adsorbents for dye removal – A review. J Environ Manage 90(8):2313–2342. https://doi.org/10.1016/j.jenvman.2008.11.017

Gurreri L, Tamburini A, Cipollina A, Micale G (2020) Electrodialysis applications in wastewater treatment for environmental protection

and resources recovery: a systematic review on progress and perspectives. Membranes 10(7):146

Hameed BH, Ahmad AL, Latiff KNA (2007) Adsorption of basic dye (methylene blue) onto activated carbon prepared from rattan sawdust. Dyes Pigm 75(1):143–149. https://doi.org/10.1016/j.dyepig.2006.05.039

Hasan SH, Ranjan D, Talat M (2010) Agro-industrial waste 'wheat bran' for the biosorptive remediation of selenium through continuous up-flow fixed-bed column. J Hazard Mater 181(1):1134–1142. https://doi.org/10.1016/j.jhazmat.2010.05.133

He L, Zhong H, Liu G, Dai Z, Brookes PC, Xu J (2019) Remediation of heavy metal contaminated soils by biochar: mechanisms, potential risks and applications in China. Environ Pollut 252:846–855. https://doi.org/10.1016/j.envpol.2019.05.151

Inyang MI, Gao B, Yao Y, Xue Y, Zimmerman A, Mosa A, Cao X (2016) A review of biochar as a low-cost adsorbent for aqueous heavy metal removal. Crit Rev Environ Sci Technol 46(4):406–433. https://doi.org/10.1080/10643389.2015.1096880

Iqbal M, Saeed A, Zafar SI (2009) FTIR spectrophotometry, kinetics and adsorption isotherms modeling, ion exchange, and EDX analysis for understanding the mechanism of Cd2+ and Pb2+ removal by mango peel waste. J Hazard Mater 164(1):161–171. https://doi.org/10.1016/j.jhazmat.2008.07.141

Kacmaz H (2020) Assessment of heavy metal contamination in natural waters of Dereli, Giresun: an area containing mineral deposits in northeastern Turkey. Environ Monit Assess 192(2):91. https://doi.org/10.1007/s10661-019-8057-0

Kinuthia GK, Ngure V, Beti D, Lugalia R, Wangila A, Kamau L (2020) Levels of heavy metals in wastewater and soil samples from open drainage channels in Nairobi, Kenya: community health implication. Sci Rep 10(1):8434. https://doi.org/10.1038/s41598-020-65359-5

Kumar U, Bandyopadhyay M (2006) Sorption of cadmium from aqueous solution using pretreated rice husk. Biores Technol 97(1):104–109. https://doi.org/10.1016/j.biortech.2005.02.027

Liu XY, Huang M, Ma HL, Zhang ZQ, Gao JM, Zhu YL, Guo XY (2010) Preparation of a carbon-based solid acid catalyst by sulfonating activated carbon in a chemical reduction process. Molecules 15:10. https://doi.org/10.3390/molecules15107188

Liu Y, Kang Y, Huang D, Wang A (2012) Cu2+ removal from aqueous solution by modified chitosan hydrogels. J Chem Technol Biotechnol 87(7):1010–1016. https://doi.org/10.1002/jctb.3722

Liu Y, Yan J, Yuan DLiQ, Wu, X, (2013) The study of lead removal from aqueous solution using an electrochemical method with a stainless steel net electrode coated with single wall carbon nanotubes. Chem Eng J 218:81–88. https://doi.org/10.1016/j.cej.2012.12.020

Liu Z, Zhang FS (2009) Removal of lead from water using biochars prepared from hydrothermal liquefaction of biomass. J Hazard Mater 167(1):933–939. https://doi.org/10.1016/j.jhazmat.2009.01.085

Lodeiro P, Herrero R, Sastre de Vicente ME (2006) Batch desorption studies and multiple sorption–regeneration cycles in a fixed-bed column for Cd(II) elimination by protonated Sargassum muticum. J Hazard Mater 137(3):1649–1655. https://doi.org/10.1016/j.jhazmat.2006.05.003

Long Y, Lei D, Ni J, Ren Z, Chen C, Xu H (2014) Packed bed column studies on lead(II) removal from industrial wastewater by modified Agaricus bisporus. Biores Technol 152:457–463. https://doi.org/10.1016/j.biortech.2013.11.039

Manasi RV, Santhana Krishna Kumar A, Rajesh N (2014) Biosorption of cadmium using a novel bacterium isolated from an electronic industry effluent. Chem Eng J 235:176–185. https://doi.org/10.1016/j.cej.2013.09.016

Mo X, López DE, Suwannakarn K, Liu Y, Lotero E, Goodwin JG, Lu C (2008) Activation and deactivation characteristics of sulfonated carbon catalysts. J Catal 254(2):332–338. https://doi.org/10.1016/j.jcat.2008.01.011

Pang FM, Kumar P, Teng TT, Mohd Omar AK, Wasewar KL (2011) Removal of lead, zinc and iron by coagulation–flocculation. J Taiwan Inst Chem Eng 42(5):809–815. https://doi.org/10.1016/j.jtice.2011.01.009

Pilli SR, Goud VV, Mohanty K (2012) Biosorption of Cr(VI) on immobilized Hydrilla verticillata in a continuous up-flow packed bed: prediction of kinetic parameters and breakthrough curves. Desalin Water Treat 50(1–3):115–124. https://doi.org/10.1080/19443994.2012.708555

Premarathna KSD, Rajapaksha AU, Sarkar B, Kwon EE, Bhatnagar A, Ok YS, Vithanage M (2019) Biochar-based engineered composites for sorptive decontamination of water: A review. Chem Eng J 372:536–550. https://doi.org/10.1016/j.cej.2019.04.097

Rajamani R, Vinoth kumar B, Sujith AKE, (2018) Activated Carbon Production from Waste Biomass. International Journal of Engineering & Technology 7:345–348

Raman, RSV (2015) *Preparation and Characterization of Activated Carbon from Waste Food Packaging Polymers.*

Rao BVSK, Chandra Mouli K, Rambabu N, Dalai AK, Prasad RBN (2011) Carbon-based solid acid catalyst from de-oiled canola meal for biodiesel production. Catal Commun 14(1):20–26. https://doi.org/10.1016/j.catcom.2011.07.011

Saadi Z, Saadi R, Fazaeli R (2013) Fixed-bed adsorption dynamics of Pb (II) adsorption from aqueous solution using nanostructured γ-alumina. J Nanostruct Chem 3(48):1–8. https://doi.org/10.1186/2193-8865-3-48

Saffaj N, Loukili H, Younssi SA, Albizane A, Bouhria M, Persin M, Larbot A (2004) Filtration of solution containing heavy metals and dyes by means of ultrafiltration membranes deposited on support made of Moroccan clay. Desalination 168:301–306. https://doi.org/10.1016/j.desal.2004.07.013

Sarin V, Singh TS, Pant KK (2006) Thermodynamic and breakthrough column studies for the selective sorption of chromium from industrial effluent on activated eucalyptus bark. Biores Technol 97(16):1986–1993. https://doi.org/10.1016/j.biortech.2005.10.001

Sultan H, Ahmed N, Mubashir M, Danish S (2020a) Chemical production of acidified activated carbon and its influences on soil fertility comparative to thermo-pyrolyzed biochar. Sci Rep 10(1):595. https://doi.org/10.1038/s41598-020-57535-4

Sultan H, Ahmed N, Mubashir M, Danish S (2020b) Chemical production of acidified activated carbon and its influences on soil fertility comparative to thermo-pyrolyzed biochar. Sci Rep 10(1):1–8

Thomas HC (1944) Heterogeneous ion exchange in a flowing system. J Am Chem Soc 66(10):1664–1666

Titirici MM (2012) Hydrothermal carbonisation: a sustainable alternative to versatile carbon materials. Universität Potsdam, Potsdam

Tsubouchi N, Xu C, Ohtsuka Y (2003) Carbon Crystallization during high-temperature pyrolysis of coals and the enhancement by calcium. Energy Fuels 17(5):1119–1125. https://doi.org/10.1021/ef020265u

UN-Water, (2020) UN World Water Development Report 2020 *Water and Climate Change*. France, Paris

Vieira MLG, Esquerdo VM, Nobre LR, Dotto GL, Pinto LAA (2014) Glass beads coated with chitosan for the food azo dyes adsorption in a fixed bed column. J Ind Eng Chem 20(5):3387–3393. https://doi.org/10.1016/j.jiec.2013.12.024

Yahaya N, Abustan I, Latiff M, Bello OS, Ahmad MA (2011) Fixed-bed column study for Cu(II) removal from aqueous solutions using rice husk based activated carbon. Int J Eng Technol 11(1):248–252

Yoon YH, Nelson JH (1984) Application of gas adsorption kinetics I. A Theoretical model for respirator cartridge service life. Am Ind Hyg Assoc J 45(8):509–516. https://doi.org/10.1080/15298668491400197

Yuan P, Wang J, Pan Y, Shen B, Wu C (2019) Review of biochar for the management of contaminated soil: Preparation, application and prospect. Sci Total Environ 659:473–490. https://doi.org/10.1016/j.scitotenv.2018.12.400

Zewail TM, Yousef NS (2015) Kinetic study of heavy metal ions removal by ion exchange in batch conical air spouted bed. Alex Eng J 54(1):83–90. https://doi.org/10.1016/j.aej.2014.11.008

Zhang Z, Zhu Z, Shen B, Liu L (2019) Insights into biochar and hydrochar production and applications: a review. Energy 171:581–598

Zhao J, Shen XJ, Domene X, Alcañiz JM, Liao X, Palet C (2019) Comparison of biochars derived from different types of feedstock and their potential for heavy metal removal in multiple-metal solutions. Sci Rep 9(1):9869. https://doi.org/10.1038/s41598-019-46234-4

Zheng P, Bai B, Guan W, Wang H, Suo Y (2016) Fixed-bed column studies for the removal of anionic dye from aqueous solution using TiO2@glucose carbon composites and bed regeneration study. J Mater Sci: Mater Electron 27(1):867–877. https://doi.org/10.1007/s10854-015-3828-z

Zhou Q, Yang N, Li Y, Ren B, Ding X, Bian H, Yao X (2020) Total concentrations and sources of heavy metal pollution in global river and lake water bodies from 1972 to 2017. Global Ecology and Conservation 22:e00925. https://doi.org/10.1016/j.gecco.2020.e00925